RSC Advances

ROYAL SOCIETY OF CHEMISTRY

www.rsc.org/advances

RSC Advances

ARTICLE

Preparation of graphene oxide with silver nanowires to enhance antibacterial properties and cell compatibility

Received 00th Aguest 2015,
Accepted 00th September 2015

DOI: 10.1039/x0xx00000x

www.rsc.org/rsc advances

Jianghu Cui,[a] Yingliang Liu, [†]

In this work, we present a simple approach for the deposition of silver nanowires onto graphene oxide sheets (GO-Ag NWs). Silver nanowires were evenly distributed and tightly adherent to the surface of graphene oxide (GO) sheets. Results from this study showed that the silver ion was released from GO sheets in a constant and slow manner. Importantly, the results showed that the antibacterial activity of GO-Ag NWs was much more potent than that of silver nanowires. Changes in cellular morphology, the level of reactive oxygen species (ROS) and the content of DNA and RNA were also investigated. It was demonstrated that cell membrane integrity was damaged, DNA, RNA and protein was leaked out due to the silver ion brought about oxidative damage towards bacteria through releasing ROS. On the basis of the present investigation, a plausible antibacterial mechanism of GO-Ag NWs composites was proposed. Lastly, the results showed that the same samples which decreased bacterial growth the most did not inhibit human skin keratinocytes cell growth compared to Ag NWs. In summary, results from this study indicated that GO-Ag NWs provided unprecedented antibacterial properties while maintaining the cell proliferation capacity necessary for enhancing the use of silver in wide medical application.

1. INTRODUCTION

With the threat of antibiotic resistant bacteria, researchers are searching for new antibacterial agents in order to control the bacteria.[1] Owing to their unique chemical and physical properties, nanoscale materials have been explored as antibacterial products and attracted the attention of many research groups worldwide.[2-4] Some types of nanomaterials like zinc oxide, [5] titanium oxide, [6] copper and its oxide,[7] silver [8] have been studied. It is well known that silver nanoparticles (Ag NPs) have become the engineered nanomaterials with the highest degree of commercialization due to their broad-spectrum antibacterial activities and the minimal resistant development.[9, 10] Although there have been plenty of investigations to explore the potential application of Ag NPs in antibacterial therapy. However, the practical application of Ag NPs is often weaken by the self-aggregation or precipitation, and lose of antibacterial activity.[11] To overcome this shortcoming, silver-based materials have been widely investigated, such as macromolecules,[12] silicon-based[13, 14] and carbon[15] materials have been used as support materials to load Ag NPs, integrating excellent antibacterial effects and the other optical, electronic and magnetic properties.

Graphene oxide (GO) has attracted broad attention in biomedical applications with unique chemical, physical and thermal properties, such as photothermal therapy agent for tumors,[16-20] cellular imaging,[21, 22] chemical and biological sensors[23, 24] and nanocarrier for drug delivery.[20, 25] Meanwhile, GO owns specific high surface area, and has a great deal of oxygen bonds in its edges and defective sites. Therefore, GO is strongly hydrophilic, and forms stable colloidal dispersions in water.[26] Such functional groups have been confirmed to own reducibility.[27] GO has been used as a highly biocompatible substrate to build new composites.[28] For example, some metal nanoparticles were employed to decorate GO sheets.[29-32] These GO-based nanocomposites with fascinating properties have attracted research attention in biomedicine.[33]

Herein, we report a simple method for the synthesis of graphene oxide loaded silver nanowires (GO-Ag NWs). The minimum inhibitory concentration, the bacterial growth kinetics and quantitative assessments of GO-Ag NWs were performed. Changes in cellular morphology, the level of reactive oxygen species (ROS) and the content of DNA and RNA were also examined. Our results showed that GO-Ag NWs could effectively enhance the antibacterial activity via ROS and release of silver ions. Taken together, this study illustrated the antibacterial activity against *Escherichiae coli* (*E. coli*) and *Staphylococcus aureus* (*S. aureus*), and provided evidences to promote the application of silver in the treatment of infectious diseases.

2. EXPERIMANTAL SECTION

2.1 Materials

Ascorbic acid and cetyltrimethylammoniun bromide (CTAB) was prepared were purchased from Guangzhou Chemical Reagent Factory. Poly (N-vinyl-2-pyrrolidone) (PVP, molecular weight = 30000-40000), graphite and $KMnO_4$ were obtained from Shanghai Chemical Factory (Shanghai, China). 2, 7-dichlorofluorescin-diacetate (DCFH-DA) was purchased from BD Biosciences (CA, USA). Silver nitrate was purchased from Beijing Chemical Reagent

[a] *Guangdong Key Laboratory of Agricultural Environment Pollution Integrated Control, Guangdong Institute of Eco-Environmental and Soil Sciences, Guangzhou 510650, China*
† College of Materials and Energy, South China Agricultural University, 510642, Guangzhou, Guangdong, P R China

Factory (Beijing, China). Others chemical reagents used in this study were of analytical grade and used without further purification. Water was purified by using the Pine-Tree system.

2.2 Preparation of graphene oxide

The water soluble GO were prepared by oxidizing pristine graphite according to the modified Hummers method.[34] The graphite powder (1 g) was placed in concentrated H_2SO_4 (98%, 23 mL) at 0 °C. $KMnO_4$ (3 g) was added gradually with stirring and keeping the temperature of the mixture below 20 °C. The mixture was then stirred at 35 °C for 2 h, followed by the addition of 46 mL distilled water and continuous stirring for 15 min. 140 mL distilled water was then added to terminate the reaction. Then, 30 % H_2O_2 (2 mL) was added and the color of the mixture changed to bright yellow. The mixture was washed by repeated centrifugation with HCl aqueous solution and distilled water. The solutions were dried in vacuum and GO powder was obtained.

2.3 Preparation of Ag NWs

Preparation of the silver seed: 20 mL of 0.25 mM $AgNO_3$ and 5 mL 0.25 mM trisodium citrate were mixed. The mixed solution was added 0.6 mL of 10 mM $NaBH_4$ and stirred vigorously all at once. Stirring was stopped after 30 s.[35] A solution containing 2.5 mL of 10 mM $AgNO_3$, 5.0 mL of 100 mM ascorbic acid and 93 mL of 80 mM cetyltrimethylammoniun bromide (CTAB) was prepared. Then, 2.5 mL of the silver seed solution was added. Finally, 0.5 mL of 1 M NaOH was added, the solution was gently shaken just enough to mix the NaOH. A yellow color appeared within 15 min. Ag NWs were collected by the addition of a large amount of distilled water, followed by sonication and centrifugation.

2.4 Preparation of GO-Ag NWs

50 mg GO powder was dissolved in 50 mL H_2O and sonicated for 30 min to form a homogeneous GO suspension. 2 g PVP was added in the GO solution and kept at 65°C for 30 min. Then, the prepared 4 mL of Ag NWs solution was rapidly added into above solution under vigorous stirring. After continued stirring for 6 h in the dark, the sample was collected and washed with deionized water three times by centrifugation, and then freeze dried for further measurements in vacuum.

2.5 Characterization

The obtained samples were characterized by X-ray diffraction (XRD) performed on a MSAL-XD2 X-ray diffractometer with Cu target in the 2θ range from 5° to 80° (40 kV, 30 mA, λ = 1.54051 Å). Morphological features of the samples were performed by field emission scanning electron microscopy (FESEM), transmission electron microscopy (TEM) and JEOL JEM-2100F field emission electron microscope equipped with an Oxford INCA Energy TEM 200 EDS system. X-ray photoelectron spectroscopy (XPS) measurement was obtained from an ESCALAB-MKII spectrometer with an Axis Ultra photoelectron spectrometer using monochromatic Mg Kα X-ray (1253.6 eV) and binding energies were referred to C1s (284.8 eV). The concentration of silver was estimated using an inductively multitype coupled plasma emission spectrometer (PerkinElmer, nexion 300).

2.6 Antibacterial Assay

In order to explore the antibacterial activities of synthesized GO-Ag NWs composites, *E. coli* and *S. aureus* were introduced and cultured in Luria-Bertani (LB) medium and incubated in a shaking incubator at 37 °C. Minimum inhibitory concentration (MIC) of GO-Ag NWs composites was measured by standardized agar dilution. Briefly, *E. coli* and *S. aureus* cells were spotted on a series of agar plates containing dilutions of the GO-Ag NWs composites and incubated at 37 °C. The MIC value is defined as the lowest concentration of GO-Ag NWs at which no visible bacterial growth is observed. For comparison, the MIC of ampicillin was also determined following the same method.

In order to further explore the antibacterial activities of synthesized GO-Ag NWs composites, approximately 1×10^8 cfu/mL cells were grown in 50 mL liquid LB medium supplemented with 12.5, 25, 50, 100 μg/mL of Ag NWs and the GO-Ag NWs composites. Pure medium without material treatment and bacteria cell inoculation were served as the negative control. Growth rates and bacterial concentrations were detected by measuring optical density (O.D.) of LB in broth medium at 600 nm each hour.

Bacteria were incubated 24 h with the samples in order to show the viability of bacteria on the samples by using fluorescence staining. GO, Ag NWs and GO-Ag NWs were added into solution to make up concentration of 10 μg $mL^{-1.}$ The culture medium was then removed and the samples were rinsed, stained using acridine orange (AO) and ethidium bromide (EB) for 15 min in dark, and observed by fluorescence microscopy. EB did not penetrate the plasma membrane in the live cells and stained only the dead cells, whereas AO penetrated the plasma membrane and stained the live and dead cells. The live cells appeared green while the dead cells were orange.

2.7 Release Property

About 10 mg of Ag NWs and GO-Ag NWs solid and the same equivalent $AgNO_3$ solution were added to 10 mL of ultrapure water and mixed into homogeneous solutions respectively. Transfer the solutions into the dialysis bags were immersed into 50 mL ultrapure water in a shaking incubator at 37 °C. After a given time interval, the concentration of silver ions was determined using an inductive coupled plasma mass spectrometer (ICP-MS).

2.8 Cell morphological change

To visualize the morphology of the test bacteria in detail after treatment with the synthesized nanocomposites, we selected 10 μg/mL of the synthesized GO-Ag NWs as the final concentration to treat the *E.coli* cells with a sterilized silicon chip in the bottom. The samples and test cells were prepared as mentioned above. Silicon chip with *E.coli* cells grown in materials-free medium was used as control. After incubated for 2 h, the silicon chip was collected and processed for scanning electron microscopy as the following the techniques. Briefly, the silicon chip was gently removed from the microtiter plates, washed three times with buffer to remove nonadherent bacteria cells and medium residue. Subsequently, the chip was fixed in 2.5% glutaraldehyde for 2 h at 4 °C. After fixation the silicon chip was rinsed with buffer, and subjected to dehydration process by replacing the buffer with a graded series of ethanol. The silicon chip was dried before the chip was attached to aluminum stub and coated by gold sputter for conductive coating. The samples were then detected under FESEM.

2.9 Leakage contents of DNA, RNA and proteins of *E. coli*

50 mL of sample was added into a certain volume of a sterile 0.5 wt % saline solution containing approximately 10^8 cfu/mL of *E. coli*. Then, the suspension was shaken for 1, 2, 3, 4, 5 and 6 h. After that, the solution was taken out and filtered by a Millipore filter. Finally, the optical density of the filtrate was recorded at 260 nm and 280 nm.

2.10 Intracellular reactive oxygen species (ROS)

To determine the intracellular generation of ROS, an intracellular ROS-indicator, DCFH-DA was used. The oxidation of non-fluorescent 2,7-dichlorofluorescin (DCFH) to highly fluorescent DCFH-DA provides a quantitative assay of ROS formation. Experimental procedures were carried out exactly as the previously described method. [36, 37] K12 Cells were exposed to the samples at the concentration of 10 μg mL^{-1} for 2 h in the dark and immediately analyzed with flow cytometry. The 488 nm laser was conducted for excitation and fluorescence was detected in FL-1. For each sample, the mean fluorescence intensity of 10,000 cells was measured to present its intracellular production of ROS.

2.11 Cytotoxicity assay

Human skin keratinocytes (HaCaT) cells were cultured in the media contained fetal bovine serum (10%), penicillin (1000 units/mL) and streptomycin (1 mg/mL) at 37 °C in a 5% CO2 humidified environment. The cell viability was evaluated by MTT assay. GO-Ag NWs and Ag NWs samples were added separately with a predetermined concentration in culture medium (6.25, 12.5, 25 and 50 μg/mL). Cells cultured in the medium without material were taken as the control. Finally, the absorbance was estimated on a Bio-Rad ELISA reader after 24, 48 and 72 h treatments.

3. RESULTS and DISCUSSION

3.1 Synthesis and characterization of GO-Ag NWs

The Ag NWs were synthesized at 160 °C for 2.5 h using a solvothermal method. Fig. 2A and B shows the FESEM images of as-prepared Ag NWs. The diameter of Ag NWs is about 50 nm, and their lengths reach up to several tens to hundreds of micrometers. No other morphology of Ag NWs was observed, the yield of Ag NWs is almost 100 % under the present synthetic conditions, and the large-scale production of Ag NWs is able to be carried out by increasing the content of $AgNO_3$ or scaling up the reaction volume. The microstructure of Ag NWs was investigated by X-ray diffraction (XRD) and high-resolution transmission electron microscopy HRTEM).Four diffraction peaks from the XRD pattern (Figure 2C) were observed and indexed to the (111), (200), (220), and (311)

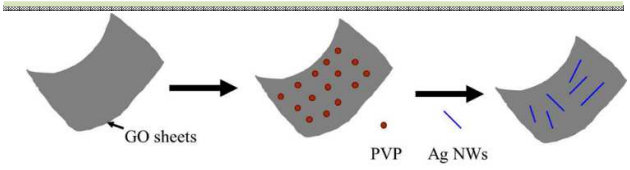

Fig. 1 Schematic representation of the reaction steps leading to the preparation of GO-Ag NWs.

(planes of face-centered-cubic silver crystals. The calculated lattice constant based on the XRD pattern is 4.09 Å, close to the reported data. Moreover, no peaks are attributed to silver oxide to indicate the purity and high quality of Ag NWs. Furthermore, in order to obtain the detailed structural information of the Ag NWs, Figure 2D shows a HRTEM image from the edge of an individual Ag NWs. The interplanar spacing for the lattice fringes is 0.23 nm, which are consistent with the plane distance of silver (111).

In order to synthesize GO-Ag NWs, we chose PVP as the reductant and stabilizer. This facile procedure was schematically illustrated in Fig. 1. PVP has been widely used in medicine due to its low toxicity, chemical stability, and good biocompatibility. [38] The as-prepared GO nanosheets were obtained using a modified Hummers method (Fig. 3A). The formation of GO-Ag NWs could be readily indicated that Ag NWs were supported on GO sheets without aggregation (Fig. 3B and C). The chemical composition of GO-Ag NWs is determined using the energy dispersive spectrum (EDS). As shown in Fig. 3F, there are several kinds of peaks in the EDS spectrum taken from GO-Ag NWs, which corresponds to carbon, oxygen, copper and silver elements, respectively. The element of copper comes from the copper grid. It confirms the existence of Ag NWs on the surface of GO sheets. GO-Ag NWs was also characterized by using XPS. From the XPS results (Fig.4A and B), the C1s line was used as a reference for the binding energy scale

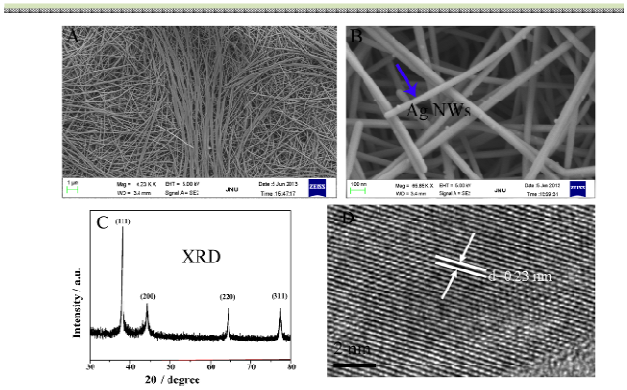

Fig. 2 FESEM images of the as-synthesized Ag NWs (A and B); XRD pattern of Ag NWs (C); HRTEM image of an individual Ag NWs (D).

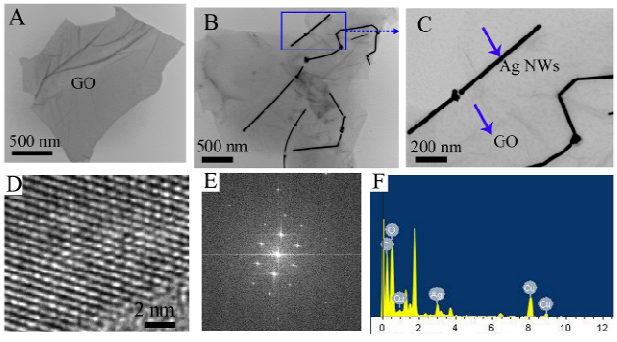

Fig. 3 TEM images of the as-synthesized GO (A) and GO-Ag NWs (B and C); (D) HRTEM image of an individual Ag NWs ; (E) SAED image of an individual Ag NWs; EDS pattern of GO-Ag NWs (F).

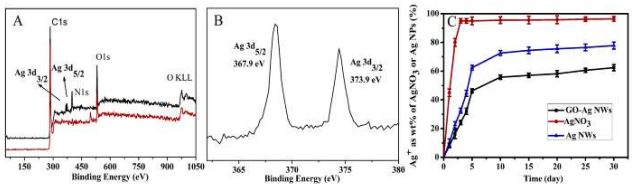

Fig. 4 XPS patterns of GO and GO-Ag NWs (A and B); Data collected for the dissolution of $AgNO_3$, Ag NWs and GO-Ag NWs at 37 °C (C).

Table 1 MIC Values of the samples against *E. coli* and *S. aureus*

bacteria	Ag NWs	GO-Ag NWs	ampicillin
E. coli	**28**	**16**	**14**
S. aureus	**35**	**20**	**12**

(284.5 eV), and the line positions of both N and O are 400 and 531 eV, respectively. Fig. 4B shows that the energy splitting value of 6.0 eV for the 3d doublet of Ag indicates the formation of metallic silver, which further supports the conclusion that the surface of GO have loaded successfully with Ag NWs. The as-prepared GO-Ag NWs contains about 6.65 wt. % Ag and 72.43 wt. % C from the result of XPS.

3.2 Release property

The release kinetics of silver ions from silver-containing antibacterial agents is a key parameter in evaluating its applicability. In this study, the releasing profiles of silver ions were analyzed by ICP. As shown in Fig. 4C, the diffusion of silver ions was very fast from $AgNO_3$ sample to the aqueous phase in the first few hours. For Ag NWs and GO-Ag NWs, the release of Ag+ out of the dialysis tube was much slower relatively compared with that of $AgNO_3$, after 30 days, approximately 77.8 % and 62.4 % Ag+ release out of the dialysis, respectively. The GO-Ag NWs showed much lower release speed than Ag NWs, which played longer antibacterial activity than that of Ag NWs. It was reported that the bacterial inactivation kinetics shows the interfacial charge transfer process[39, 40].The silver ions from this nanocomposites may be exchanged with hydronium ions in the fluid phase, whereas the release of silver ions from Ag NWs anchored in GO can be delayed by the diffusion rate of silver ions from the surface of GO.

3.3 Antibacterial measurements

The susceptibilities of *E. coli* and *S. aureus* to the GO-Ag NWs nanocomposite were demonstrated by the MIC value, an important parameter to evaluate the bacterial susceptibility to a certain antibacterial agent. As shown in Table 1, no visible *E. coli* growth can be observed on agar plates containing as low as 16 μg/mL of GO-Ag NWs, while 20 μg/mL of GO-Ag NWs is required to completely inhibit the growth of *S.aureus*, indicating that *E. coli* is more susceptible to GO-Ag NWs than *S. aureus*. Interestingly, when compared to antibiotics, the MIC of ampicillin against *S. aureus* is lower than GO-Ag NWs, whereas in the case of *E. coli*, the MIC of GO-Ag NWs is equivalent. These large differences variations of MIC between different bacteria species and antibacterial materials could indicate their distinct antibacterial mechanisms. The as-synthesized GO-Ag NWs nanocomposites are inorganic materials, with equivalent antibacterial efficiency in comparison to that of ampicillin, and they should be widely used in the medical application field as an alternative antibacterial material.

Antibacterial activity of the samples is further studied through measurements of the optical density of the sample and growth observation of using E.coli. The rate and extent of growth inhibition can be determined from time dependency of recorded growth of the testing K12 cells during 24 h cultivation. Given the advanced structure of the GO-Ag NWs, we performed antibacterial assaysby measuring the effects of GO-Ag NWs on the bacterial growth kinetics in liquid media in the absence of light based on the turbidity of the cell suspension.

Fig. 5A shows that GO alone has no obvious inhibition on bacteria growth even at a high concentration. However, the growth of bacterial cells was completely inhibited in the presence of GO-Ag NWs (>25 μg/mL). The time-dependence study of the growth inhibition of bacteria cells confirmed higher sensitivity of E.coli to GO-Ag NWs than that of Ag NWs (Fig. 5B and C). As a traditional antibiotic, ampicillin has excellent antibacterial properties, but its instability limits its application. However, the as-synthesized GO-Ag NWs composites are inorganic materials with stable properties, with equivalent antibacterial efficiency in comparison to that of ampicillin, and they should be widely used in the medical application as an

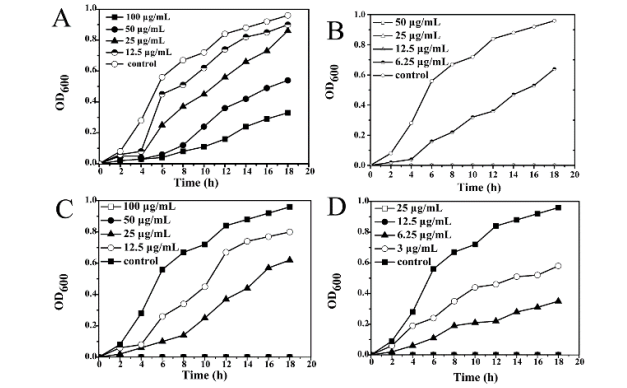

Fig. 5 Growth curves of *E.coli* was inhibited by GO (A), GO-Ag NWs (B), Ag NWs (C) and ampicillin (D).

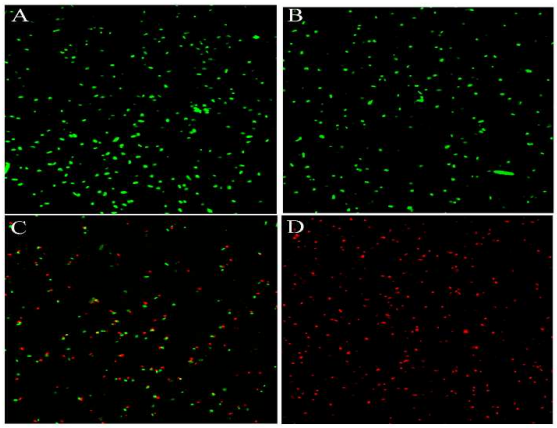

Fig. 6 Representative images showing viability of the bacteria on the control (A), GO (B), Ag NWs (C) and GO-Ag NWs (D) after 2 h of incubation displayed by AO and EB fluorescence staining.

alternative antibacterial material. The ability of GO-Ag NWs to prevent viable bacteria colonization is also demonstrated by fluorescence staining. As shown in Fig. 6, the results suggest that almost all of bacteria are viable when cultured on the control and GO.There are large amounts of viable bacteria on Ag NWs and smaller amounts on GO-Ag NWs.

3.4 Cell morphological change with GO-Ag NWs treatment

To understand the antibacterial mechanism, the interaction of GO-Ag NWs composite with *E. coli* bacteria and the morphological change in *E. coli* cells was evaluated by FESEM. Fig. 7(A) and (B) shows the FESEM images of *E. coli* cells untreated and treated with GO-Ag NWs. It is observed that there are no significant morphological changes in the untreated *E. coli* cells and the cell membranes kept relative integrity (Fig. 7A). However, the cells treated with GO-Ag NWs exhibited apparently morphological changes, and the structure of the cell walls treated with GO-Ag NWs showed significant damage. The disruption of the integrity of the cell membrane leads to lysis of the internal cell structure, as shown in Fig. 7B. Our antibacterial experiments demonstrate that the GO-Ag NWs exhibit enhanced antibacterial activity in both *E. coli* and *S. aureu*.

In our work, Ag NWs have been loaded onto the surface of the GO to effectively prevent their aggregation and protect their high surface reactivity. In addition, the GO has stronger adsorption properties due to bind and be in close proximity to the bacterial surface. GO-Ag NWs could more tend to stimulate the production of ROS, and thereby leading to the disruption of the integrity of the cell membrane and cell death. Thus, the as-synthesized nanocomposites are highly efficient inhibitors of bacterial growth.

3.5 Leakage contents of DNA, RNA and proteins of *E. coli*

In order to study the antibacterial effect of GO-Ag NWs nanocomposite, the content of DNA, RNA and protein from the untreated and treated *E. coli* cells were analyzed. DNA and RNA have an ultraviolet absorption peak at approximately 260 nm due to the conjugated double bond system between purine ring and pyrimidine ring, while protein has an ultraviolet absorption peak at approximately 280 nm because of the existence of a conjugated double bond system between tyrosine and tryptophan. Hence, the influence of DNA, RNA and protein corresponding to *E. coli* treated with GO-Ag NWs nanocomposite could be analyzed by measuring the O.D. values at 260 nm and 280 nm, respectively. As seen from the results (Figure 8A and B), after the contact between the *E. coli* and the samples, the higher antibacterial activities of GO-Ag NWs would result in more leakage of DNA, RNA and protein at the same treated time. Moreover, the content of DNA, RNA and protein all gradually decreased with a prolonged contact time. Meanwhile, we

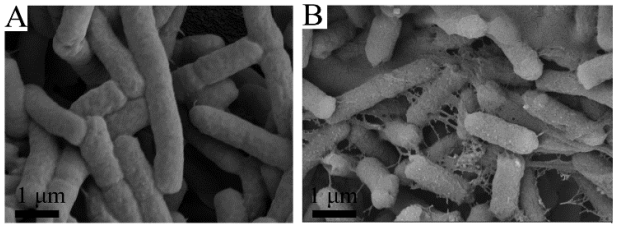

Fig. 7 FESEM images about the surface morphology of *E. coli* were treated with control (A) and GO-Ag NWs (B).

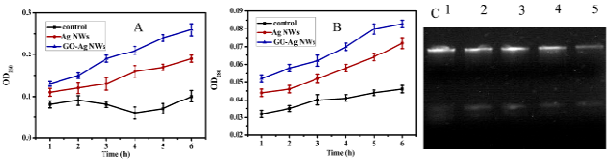

Fig. 8 Leakage contents of (A) DNA and RNA and protein (B) of *E. coli*; (C) Effect of GO-Ag NWs nanocomposites on plasmid DNA. Lane 1 represents plasmid DNA isolated from untreated *E.coli*, Lane 2 , 3, 4 and 5 represents plasmid DNA isolated from *E.coli* treated with 5 μg/mL and 10 μg/mL Ag NWs and GO-Ag NWs, respectively.

investigate the antibacterial effect of GO-Ag NWs nanocomposite, the DNA isolated from the untreated and treated *E. coli* cells were analyzed by agarose gel electrophoresis. The results indicate that the intensity of DNA band in lane 2 and 3 corresponding to *E. coli* treated with 5 μg/mL and 10 μg/mL of Ag NWs was no change as compared to control DNA in lane 1, suggests that Ag NWs exert no considerable effects on the plasmid DNA replication. *E. coli* treated with 5 μg/mL and 10 μg/mL of GO-Ag NWs suggests that the concentration of lane 4 and 5 DNA is obviously lower than the control due to GO-Ag NWs exert considerable effects on the plasmid DNA replication. FESEM (Fig. 7) and electrophoretic results show the dual-mode antibacterial effect of the GO-Ag NWs by damaging cell membrane and inhibiting DNA replication results in bacterial cell death.

3.6 Reactive oxygen species

A large number of investigators have reported that silver nanomaterials generate ROS to impact bacterial growth.[41, 42] Increased intracellular ROS will perturb the redox potential equilibrium, bring about an intracellular pro-oxidant environment and result in a series of adverse effects.[43] To figure out the possible antibacterial mechanism of the GO-Ag NWs, we performed the level of ROS using a DCFH-DA probe, which can be hydrolyzed to the non-fluorescent DCFH by esterase in cells and can further be oxidized to produce the fluorescent dichorofluorescein (DCF) by cellular ROS.

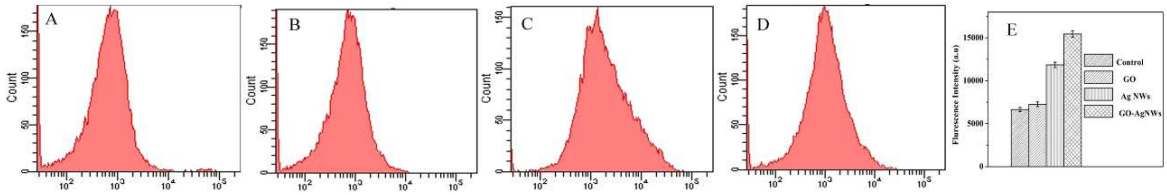

Fig. 9 Formation of ROS in *E. coli* K12 cells after 2 h incubation with Control (A), GO (B), Ag NWs (C) and GO-Ag NWs (D), respectively.

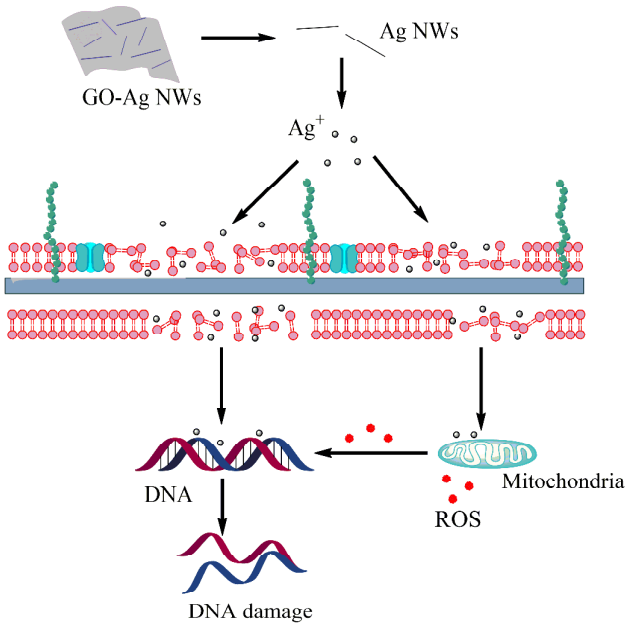

Fig 10. Schematic illustration of antibacterial mechanism of GO-Ag NWs composites.

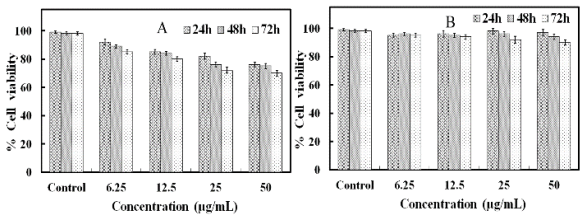

Fig. 11 Concentration-dependent in vitro toxicity of Ag NWs (A) and GO-Ag NWs (B) after 24, 48 and 72h.

Here, we investigated the oxidative stress response of Ag NWs, GO and GO-Ag NWs. ROS production is detected by flow cytometry after 2 h exposure to these samples. As shown in Fig. 9, the incubation of GO lead to slight increase in DCF fluorescence. In comparison, the DCF fluorescence intensity increases obviously with the treatment of Ag NWs and GO-Ag NWs for bacteria. ROS were detected by fluorescence measurement of the reporter DCF. All tests were repeated three times to get the mean values and standard deviations.

Compared to the Ag NWs treated cells, those treated with GO-Ag NWs were higher fluorescence intensity. The results showed that GO-Ag NWs could more tend to stimulate the production of ROS and ultimately result in a series of adverse effects on these bacterial cells. It indicates that the GO-Ag NWs can cause rupture of *E. coli* cells. The presence of nanoparticles in suspension would ensure continuous release of ions into the nutrient media. Silver ions released by the nanoparticles may have attached to the negatively charged bacterial cell walls and ruptured them, thereby leading to protein denaturation and cell death.

3.7 Effect of GO-Ag NWs on cell viability

To explore the toxicity of GO-Ag NWs material, we used the MTT assay method to measure the relative cell viability. HaCaT cells were chosen due to the likely contact of material with the skin. Fig. 11 shows the viability of untreated cells was assumed be 100%. The GO-Ag NWs were less toxic than Ag NWs at almost all dosages. Increasing the concentration of Au NPs solutions up to 50 μg/mL causes a significant increase in the toxicity and the cell viability is only 70.2%. In contrast, the cell viability for the GO-Ag NWs material is above 90%. These results indicate that the prepared GO-Ag NWs material is much more biocompatible than GO-Ag NWs.

According to the above results, we proposed the antibacterial mechanism GO-Ag NWs material as follows(Fig 10): GO-Ag NWs could interact directly with the bacterial cell membrane through electrostatic interaction and the Ag ions were transported to the cytoplasm, which caused generation of reactive oxygen species and inhibition of genomic DNA replication. The integrity of cell wall/membrane studies further demonstrated that the wall/membrane was damaged.

4. CONLUSIONS

In summary, we developed a route to deposit silver nanowires on the GO surface. This material was characterized by XRD, TEM and XPS measurements. The results indicated that Ag NWs were loaded successfully on the surfaces of GO sheets. We also confirmed that GO-Ag NWs exhibited enhanced antibacterial activities, which was caused by generation of ROS with bacteria, durative slow-releasing of silver ions and self- aggregation. In addition, the antibacterial mechanism of GO-Ag NWs was studied. GO-Ag NWs could release Ag ions that generated ROS, leading to leakage of DNA, RNA and protein, which contributed to enhance antibacterial activity From the clinical practical viewpoint, the GO-Ag NWs maybe own more promising application in clinical treatment, especially for the increasing resistances strains in clinical.

AUTHOR INFORMATION

Corresponding Author

*E-mail: tliuyl@scau.edu.cn.

Notes

The authors declare no competing financial interest.

ACKNOWLEDGEMENTS

This work was supported by the National Natural Science Foundation of China (Grant No. 41401564), Natural Science Foundation of Guangdong Province, China (No. 2014A030313706) and Science and Technology Program of Guangzhou, China (No.201510010259).

REFERENCES

1. H. Goossens, M. Ferech, R. Vander Stichele and M. Elseviers, *The Lancet*, 365, 579-587.
2. L. Zhao, H. Wang, K. Huo, X. Zhang, W. Wang, Y. Zhang, Z. Wu and P. K. Chu, *Biomaterials*, 2013, 34, 19-29.
3. M. I. Mejía, G. Restrepo, J. M. Marín, R. Sanjines, C. Pulgarín, E. Mielczarski, J. Mielczarski and J. Kiwi, *ACS Applied Materials & Interfaces*, 2010, 2, 230-235.

4. K. Page, R. G. Palgrave, I. P. Parkin, M. Wilson, S. L. P. Savin and A. V. Chadwick, *Journal of Materials Chemistry*, 2007, 17, 95-104.
5. J. T. Seil and T. J. Webster, *Acta Biomaterialia*, 2011, 7, 2579-2584.
6. K. Huo, X. Zhang, H. Wang, L. Zhao, X. Liu and P. K. Chu, *Biomaterials*, 2013, 34, 3467-3478.
7. S. Chen, Y. Guo, S. Chen, H. Yu, Z. Ge, X. Zhang, P. Zhang and J. Tang, *Journal of Materials Chemistry*, 2012, 22, 9092-9099.
8. D. Guo, L. Zhu, Z. Huang, H. Zhou, Y. Ge, W. Ma, J. Wu, X. Zhang, X. Zhou, Y. Zhang, Y. Zhao and N. Gu, *Biomaterials*, 2013, 34, 7884-7894.
9. R. Wang, L. Wang, L. Zhou, Y. Su, F. Qiu, D. Wang, J. Wu, X. Zhu and D. Yan, *Journal of Materials Chemistry*, 2012, 22, 15227-15234.
10. E. I. Alarcon, K. Udekwu, M. Skog, N. L. Pacioni, K. G. Stamplecoskie, M. González-Béjar, N. Polisetti, A. Wickham, A. Richter-Dahlfors, M. Griffith and J. C. Scaiano, *Biomaterials*, 2012, 33, 4947-4956.
11. R. Kumar and H. Münstedt, *Biomaterials*, 2005, 26, 2081-2088.
12. M. A. Nassar and A. M. Youssef, *Carbohydrate Polymers*, 2012, 89, 269-274.
13. Y. Zhou, X. Jiang, J. Tang, Y. Su, F. Peng, Y. Lu, R. Peng and Y. He, *Journal of Materials Chemistry B*, 2014, 2, 691-697.
14. A. Szegedi, M. Popova, K. Yoncheva, J. Makk, J. Mihaly and P. Shestakova, *Journal of Materials Chemistry B*, 2014, 2, 6283-6292.
15. J. Cui, C. Hu, Y. Yang, Y. Wu, L. Yang, Y. Wang, Y. Liu and Z. Jiang, *Journal of Materials Chemistry*, 2012, 22, 8121-8126.
16. O. Akhavan, E. Ghaderi, S. Aghayee, Y. Fereydooni and A. Talebi, *Journal of Materials Chemistry*, 2012, 22, 13773-13781.
17. J. T. Robinson, S. M. Tabakman, Y. Liang, H. Wang, H. S. Casalongue, V. Daniel and H. Dai, *Journal of the American Chemical Society*, 2011, 133, 6825-6831.
18. K. Yang, J. Wan, S. Zhang, B. Tian, Y. Zhang and Z. Liu, *Biomaterials*, 2012, 33, 2206-2214.
19. K. Yang, S. Zhang, G. Zhang, X. Sun, S.-T. Lee and Z. Liu, *Nano Letters*, 2010, 10, 3318-3323.
20. W. Zhang, Z. Guo, D. Huang, Z. Liu, X. Guo and H. Zhong, *Biomaterials*, 2011, 32, 8555-8561.
21. K. Liu, J.-J. Zhang, F.-F. Cheng, T.-T. Zheng, C. Wang and J.-J. Zhu, *Journal of Materials Chemistry*, 2011, 21, 12034-12040.
22. X. Sun, Z. Liu, K. Welsher, J. T. Robinson, A. Goodwin, S. Zaric and H. Dai, *Nano Research*, 2008, 1, 203-212.
23. V. Dua, S. P. Surwade, S. Ammu, S. R. Agnihotra, S. Jain, K. E. Roberts, S. Park, R. S. Ruoff and S. K. Manohar, *Angewandte Chemie-International Edition*, 2010, 49, 2154-2157.
24. J. T. Robinson, F. K. Perkins, E. S. Snow, Z. Wei and P. E. Sheehan, *Nano Letters*, 2008, 8, 3137-3140.
25. L. Zhang, J. Xia, Q. Zhao, L. Liu and Z. Zhang, *Small*, 2010, 6, 537-544.
26. R. Pasricha, S. Gupta, A. G. Joshi, N. Bahadur, D. Haranath, K. N. Sood, S. Singh and S. Singh, *Materials Today*, 2012, 15, 118-125.
27. H.-P. Cong, J.-J. He, Y. Lu and S.-H. Yu, *Small*, 2010, 6, n/a-n/a.
28. J. Zhang, F. Zhang, H. Yang, X. Huang, H. Liu, J. Zhang and S. Guo, *Langmuir*, 2010, 26, 6083-6085.
29. C. Xu, X. Wang and J. Zhu, *The Journal of Physical Chemistry C*, 2008, 112, 19841-19845.
30. C. Xu and X. Wang, *Small*, 2009, 5, 2212-2217.
31. S.-M. Paek, E. Yoo and I. Honma, *Nano Letters*, 2009, 9, 72-75.
32. C. Xu, X. Wang, L. Yang and Y. Wu, *Journal of Solid State Chemistry*, 2009, 182, 2486-2490.
33. W.-P. Xu, L.-C. Zhang, J.-P. Li, Y. Lu, H.-H. Li, Y.-N. Ma, W.-D. Wang and S.-H. Yu, *Journal of Materials Chemistry*, 2011, 21, 4593-4597.
34. J. Zhang, G. Shen, W. Wang, X. Zhou and S. Guo, *Journal of Materials Chemistry*, 2010, 20, 10824-10828.
35. N. R. Jana, L. Gearheart and C. J. Murphy, *Chemical Communications*, 2001, DOI: 10.1039/b100521i, 617-618.
36. M. C. Serrano, R. Pagani, M. Manzano, J. V. Comas and M. T. Portoles, *Biomaterials*, 2006, 27, 4706-4714.
37. S. Kim, W.-K. Oh, Y. S. Jeong, J.-Y. Hong, B.-R. Cho, J.-S. Hahn and J. Jang, *Biomaterials*, 2011, 32, 2342-2350.
38. X. Liu, Y. Xu, Z. Wu and H. Chen, *Macromolecular Bioscience*, 2013, 13, 147-154.
39. S. Rtimi, R. Sanjines, C. Pulgarin, A. Houas, J. C. Lavanchy and J. Kiwi, *Journal of Hazardous Materials*, 2013, 260, 860-868.
40. S. Rtimi, M. Pascu, R. Sanjines, C. Pulgarin, M. Ben-Simon, A. Houas, J. C. Lavanchy and J. Kiwi, *Applied Catalysis B: Environmental*, 2013, 138–139, 113-121.
41. H.-L. Su, C.-C. Chou, D.-J. Hung, S.-H. Lin, I. C. Pao, J.-H. Lin, F.-L. Huang, R.-X. Dong and J.-J. Lin, *Biomaterials*, 2009, 30, 5979-5987.
42. H.-L. Su, S.-H. Lin, J.-C. Wei, I. C. Pao, S.-H. Chiao, C.-C. Huang, S.-Z. Lin and J.-J. Lin, *PLoS ONE*, 2011, 6, e21125.
43. C. Carlson, S. M. Hussain, A. M. Schrand, L. K. Braydich-Stolle, K. L. Hess, R. L. Jones and J. J. Schlager, *The Journal of Physical Chemistry B*, 2008, 112, 13608-13619.

Captions for Figures

Fig. 1 Schematic representation of the reaction steps leading to the preparation of GO-Ag NWs.

Fig. 2 FESEM images of the as-synthesized Ag NWs (A and B); XRD pattern of Ag NWs (C); HRTEM image of an individual Ag NWs (D).

Fig. 3 TEM images of the as-synthesized GO (A) and GO-Ag NWs (B and C); (D) HRTEM image of an individual Ag NWs ; (E) SAED image of an individual Ag NWs; EDS pattern of GO-Ag NWs (F).

Fig. 4 XPS patterns of GO and GO-Ag NWs (A and B); Data collected for the dissolution of $AgNO_3$, Ag NWs and GO-Ag NWs at 37 °C (C).

Fig. 5 Growth curves of *E.coli* was inhibited by GO (A), GO-Ag NWs (B), Ag NWs (C) and ampicillin (D).

Table 1 MIC Values of the samples against *E. coli* and *S. aureus*

Fig. 6 Representative images showing viability of the bacteria on the control (A), GO (B), Ag NWs (C) and GO-Ag NWs (D) after 2 h of incubation displayed by AO and EB fluorescence staining.

Fig. 7 FESEM images about the surface morphology of *E. coli* were treated with control (A) and GO-Ag NWs (B).

Fig. 8 Leakage contents of (A) DNA and RNA and (B) protein of *E. coli*; (C) Effect of GO-AgNWs nanocomposites on plasmid DNA. Lane 1 represents plasmid DNA isolated from untreated *E.coli*, Lane 2 , 3, 4 and 5 represents plasmid DNA isolated from *E.coli* treated with 5 µg/mL and 10 µg/mL Ag NWs and GO-AgNWs, respectively.

Fig. 9 Formation of ROS in *E. coli* K12 cells after 2 h incubation with Control (A), GO (B), Ag NWs (C) and GO-Ag NWs (D), respectively. ROS were detected by fluorescence measurement of the reporter DCF. All tests were repeated three times to get the mean values and standard deviations.

Fig 10. Schematic illustration of antibacterial mechanism of GO-Ag NWs composites.

Fig. 11 Concentration-dependent in vitro toxicity of Ag NWs (A) and GO-Ag NWs (B) after 24, 48 and 72h.